Simulation of Slow Reaction with Quantum Character: Neutral Hydrolysis of Carboxylic Ester

MARC F. LENSINK,[1,2] JANEZ MAVRI,[2,3] HERMAN J. C. BERENDSEN[2]

[1] *Centre Européen de Calcul Atomique et Moléculaire (CECAM), Ecole Normale Supérieure de Lyon, 46 Allée d'Italie, 69364 Lyon cedex 07, France*

[2] *BIOSON Research Institute, Department of Biophysical Chemistry, the University of Groningen, Nijenborgh 4, 9747 AG Groningen, The Netherlands*

[3] *National Institute of Chemistry, P.O.B. 30, Hajdrihova 19, 61115, Ljubljana, Slovenia*

Received 6 July 1998; accepted 27 January 1999

ABSTRACT: By computer simulation, using both quantum and classical dynamics, we determined the rate constant and the kinetic isotope effect of the rate-determining step in the neutral hydrolysis of *p*-methoxyphenyl dichloroacetate in aqueous solution. This step involves a proton transfer concerted with the formation of a C—O bond. A method of biased sampling was used; the Gibbs free energy of the biased configuration from which proton transfer is likely to occur was determined by a combination of semiempirical quantum calculations and thermodynamic integration. The proton dynamics was modeled with the quantum-dynamical density matrix evolution method that includes nonadiabatic pathways. The proton dynamics is driven by a fluctuating proton potential that was derived from a classical molecular dynamics simulation of the system including solvent. The calculated rate constant of 3×10^{-2} s^{-1} agrees within the error of the calculation with the experimentally observed value of 2.78×10^{-3}. The calculated pseudo-first-order kinetic isotope effect of 3.9 is in good agreement with the experimentally observed value of 3.2. The results show the feasibility of computational approaches to slow reactions in complex environments, where proton transfer with an essential quantum-dynamical nature is the rate-limiting step. © 1999 John Wiley & Sons, Inc. J Comput Chem 20: 886–895, 1999

Keywords: nonadiabatic quantum dynamics; molecular dynamics; proton transfer; ester hydrolysis

Correspondence to: H. J. C. Berendsen; e-mail: berendsen@chem.rug.nl

CCC 0192-8651 / 99 / 080886-10

Introduction

Ester or amide bond cleavage by hydrolysis is a process that occurs in many enzymatic reactions. The total reaction consists of a cascade of events in which proton transfers over hydrogen bonds are important subprocesses and in many cases even form the rate-determining steps.[1] It is a challenge to present-day computational techniques to simulate such a reaction, combining the simulation of a slow, activated event with the simulation of a proton transfer with essential quantum-dynamical nature. In this article we describe the calculation of the proton transfer rate in the neutral hydrolysis of an ester in water that proceeds on a time scale of several minutes.

Normal ester bond cleavage by hydrolysis can occur rapidly in acidic or basic solution, but it is unmeasurably slow in neutral solution for simple esters like ethyl acetate. However, neutral hydrolysis can proceed in minutes in appropriately substituted esters (e.g., containing an electrophilic group such as dichloromethyl) combined with the presence of a strong leaving group. We chose to study the neutral ester bond hydrolysis of *p*-methoxyphenyl dichloroacetate in water, a well-documented reaction that has a pseudo-first-order rate constant k of $(2.78 \pm 0.06) \times 10^{-3}$ s^{-1} at 298 K and a primary deuterium kinetic isotope effect (KIE) of 3.24.[2] It has been proposed that the reactive complex (see Fig. 1) contains two water molecules and that the rate-limiting step in the neutral hydrolysis reaction is proton transfer between these water molecules concerted with the formation of a tetrahedral intermediate.[2]

In this article we compute the rate constant of the concerted reaction as follows:

1. we investigate the Born–Oppenheimer hypersurface of the reactive complex by semiempirical quantum mechanics (QM);
2. we choose proper reaction coordinates and select the reactant configuration (activated state) from which proton transfer is probable;
3. we compute the probability of that activated state in an aqueous environment by thermodynamic integration (TI)[3] based on restrained molecular dynamics simulations (MD);
4. we calculate the initial rate constant of the proton and deuteron transfer reaction in the activated state by the quantum-dynamical method of density matrix evolution (DME),[4] which uses time-dependent proton potentials derived from MD; and
5. we combine the results to obtain the initial overall reaction rate.

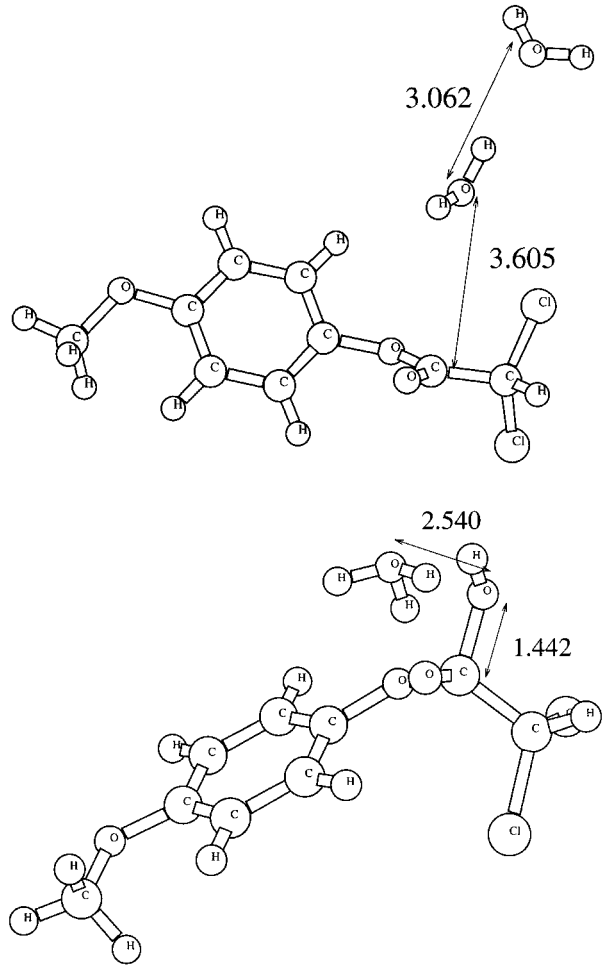

FIGURE 1. Structure of *p*-methoxyphenyl dichloroacetate with two water molecules corresponding to the (a) reactant state and (b) product state. AM1 *in vacuo* optimizations were performed under the constraint of a linear water–water hydrogen bond; the oxygen atom of the nearest water molecules was constrained to be above the carbonyl carbon atom, perpendicular to the plane defined by atoms COO constituting the ester bond. The O—H bond lengths of the hydronium ion were constrained to their AM1 calculated value of 1.004 Å. The R_{CO}, R_{OO}, and R_{OH} distances changed from 3.605 to 1.442 Å, 3.062 to 2.540 Å, and 0.963 to 1.536 Å, respectively.

For reasons of clarity, we present theory and computational results together for each of the steps mentioned above. Computational details are given in the following section.

Because of the many orders of magnitude involved in the different multiplicative contributions to k, we prefer to express the contributions in powers of 10 as $\log(k/s^{-1})$. The experimental value of $\log k$ is -2.56 ± 0.01.

To our knowledge only a few studies of reactive systems in the condensed state have been published that combine classical dynamical simulations with nonadiabatic quantum dynamics of nuclear coordinates. Most studies concern model systems or appropriately chosen systems with small activation barriers.[5,6] New approaches include surface hopping,[7] real-time path integral methods[8] and centroid dynamics,[9] and a nonadiabatic quantum transition state method to simulate infrequent events.[10] The effects of the environment on the Gibbs free energy of transition states[11] and on proton potentials[12] and dynamics[13] in enzymes were considered. Static solvent effects were included in semiempirical molecular orbital (MO) calculations on basic carboxylic ester bond cleavage[14] using a solvent reaction field.[15] Possible proton transfer paths in enzyme carbonic anhydrase were investigated using *ab initio* techniques.[16] DME was applied to proton transfer in hydrogen malonate.[17,18] Proton transfer from water to histidine in phospholipase A_2 was studied by wave-packet evolution of the proton, embedded in an empirical valence bond MD simulation.[19] Except for ref. 10, none of these studies combined quantum-dynamical proton transfer with an activated reactive step.

The essential quantum-dynamical feature of proton transfer is that nonadiabatic processes (i.e., transitions between different protonic quantum levels) may take place because the level separation is neither large enough compared to thermal energies to justify an adiabatic nor small enough to justify a classical treatment. Such transitions are driven by fluctuating interactions with the dynamic environment and must be treated by proper nonadiabatic quantum-dynamical methods. The electrons can still be adequately treated in the Born–Oppenheimer limit.

Computational Details

For semiempirical QM calculations the programs MOPAC and MOBOSOL[20] were used. *Ab initio* calculations were carried out with the program Gaussian.[21]

For classical MD simulations the GROMOS package[22] was used with the SPC water model.[23] The system consisted of a periodic box with 510 water molecules that was coupled to a temperature bath at 298 K and pressure bath at 1 bar with coupling constants of 50 fs.[24] Hydrogen atoms of the ester were treated explicitly and had small repulsive Lennard–Jones potentials on them. Bonds involving hydrogen atoms were constrained using the SHAKE algorithm.[25] A twin-range cutoff of 8 and 10 Å was employed, and the pair list was updated every 10 steps. A time step of 1 fs was used for the integration of the equations of motion using the leap-frog Verlet algorithm. Partial atomic charges for the solute were determined by fitting them to the electrostatic potential in a solvent reaction field (AM1-SM1)[26] and to the calculated dipole moment, using the Bessler–Merz–Kollman procedure.[27] For the path from reactant (R) configuration to biased configuration ($*$ state in later section) linear interpolation was used between these two states, and between the $*$ state and the product configuration (P) charges were determined by cubic spline interpolation using two additional intermediate points.

During TI the system was moved from the $*$ configuration ($\lambda = 1$) to the R configuration ($\lambda = 0$) for six fixed values of λ. Each run consisted of a 25-ps equilibration starting from the previous run (50 ps for the initial run), followed by a 50-ps simulation. The values of $dG/d\lambda$ were integrated with the extended trapezoidal rule to obtain ΔG. Errors were estimated by dividing each run into two halves and considering the variance of the distribution of all 64 combinations of the 12 derivatives. Using only the first halves of the six runs or only the second halves gave the same result within the statistical error, indicating that sufficient equilibration had taken place.

DME was carried out for a period of 12 ps, starting at time origins that were each 100 fs after the previous one and using a time step of 0.1 fs. The time-dependent Schrödinger equation was solved using 750 different time origins. Thus, a total of 87 ps of the proton potentials obtained from the MD simulation (see also later section) was in fact used. In each DME solution the density matrix was set initially to exclusive population of the ground state (corresponding to the reactant state) with off-diagonal elements set to zero, implying unknown phase information. Five simple Gaussian basis functions were used to describe the proton. These were optimized to have their first three energy levels correspond with the true energy levels of the proton in the average proton

potential. This level of description is adequate to include tunneling and nonadiabicity.[18]

Neutral Hydrolysis Reaction

We first give a short qualitative description of the succession of events in the neutral hydrolysis of an ester in aqueous solution in order to derive the necessary computational steps. We divide our system (Fig. 1a, reactant state; b, product state) into three subsystems: solvent (water), solute (ester complexed with two water molecules), and the proton. The proton transfer, together with the simultaneous electron distribution rearrangement, in the rate-limiting step can only take place when the heavy-atom configuration (with the proton in the reactant state) happens to be favorable for these concerted reactions (i.e., when the nuclear geometry is close to that of the product state, the tetrahedral intermediate depicted in Fig. 1b). In this improbable nuclear configuration the fluctuating potential felt by the proton, which is mainly due to the electric field of water molecules, causes the proton to transfer to the product side of the hydrogen bond. The tetrahedral intermediate, which may become further stabilized by solvent reorganization, subsequently dissociates irreversibly into products, picking up a proton in the process, while the hydronium ion diffuses away.

Born–Oppenheimer Surface of Reactant and Product

Due to its size, the solute does not easily allow for repeated high-level *ab initio* calculations. It was therefore treated with the AM1 semiempirical MO method, which was proven to be successful for obtaining the energetics of organic reactions with accuracies in the 1–2 kcal/mol range.[28]

The geometries of the reactant and product configurations were both optimized *in vacuo* (see Fig. 1). It was found that, apart from the proton position, the only significant changes occurred for the carbonyl carbon–water oxygen distance R_{CO} and the distance between the two water oxygens R_{OO}, which were chosen to represent the *biasing* coordinates. (In fact, there are three reaction coordinates: R_{CO}, R_{OO}, and R_{OH}; we refer to R_{CO} and R_{OO} as the biasing coordinates, while R_{OH} is the pure reaction coordinate.)

The heat of formation for the reactant and product configurations was calculated for several values of these two coordinates and was found to be 46.9 kcal/mol higher for the relaxed product state than for the relaxed reactant state. This *in vacuo* difference was smallest for a shortened CO bond and appeared to depend much more strongly on R_{CO} than on R_{OO}. The potential wells of the relaxed reactant and product states were approximated by fitting to two harmonic oscillators: the force constants for R_{CO} and R_{OO} were, respectively, 67.2 and 9.0 kcal mol^{-1} Å^{-2} in the relaxed reactant state and 973 and 101 kcal mol^{-1} Å^{-2} in the relaxed product state. The larger force constants in the product state indicate the covalent character of the CO bond and the strong ionic bond to the hydronium ion.

The semiempirical data were checked by *ab initio* calculations at the Hartree–Fock (HF)/6-31G* level and using density functional theory (DFT) for selected AM1-generated configurations. Depending on the level of theory, energy differences between product and initial state were higher than the AM1 results by 5 (DFT) to 20 (HF) kcal/mol, depending on the chosen method and basis set. This is partly due to the fact that the configurations were not relaxed in the *ab initio* calculations but is mostly due to the intrinsic incompatibility between *ab initio* methods and methods that are parametrized to reproduce experimental results. Mainly because of the computational cost of the *ab initio* methods, we chose to use the semiempirical values for further analysis and for construction of the time-dependent proton potentials (see later section).

Biased State for Proton Transfer and Its Probability

It was found that the QM energies were relatively insensitive to R_{OO}, suggesting that only the constraint of a shortened CO bond would suffice. However, it is likely that the probability of proton transfer itself depends strongly on R_{OO}. Rather than performing several quantum-dynamical simulations for different R_{OO}, we estimated the proton potential at the AM1-SM1 level with a shortened CO bond for different values of R_{OO}. The results showed a significantly lower energy barrier for a shortened R_{OO} coordinate, which strongly

suggests that the biased form of choice is the one where R_{OO} also has its product value. This is indeed the configuration used in this work.

Separating the two degrees of freedom $r_1 = R_{CO}$ and $r_2 = R_{OO}$ as the *biasing coordinate plane*, the probability for the system to reside in a surface element $dr_1 dr_2$ on this plane is proportional to $\exp(-\Delta G_{mf}(r_1, r_2)/RT)\, dr_1 dr_2$, where $\Delta G_{mf}(r_1, r_2)$ is the *potential of mean force* and equilibration over all other degrees of freedom is assumed. ΔG_{mf} is arbitrarily chosen to be zero at the bottom of the potential well in the reactant state. The probability of being in the reactant state is proportional to the integral of $\exp(-\Delta G_{mf}(r_1, r_2)/RT)$ over a region of the biasing coordinate plane that covers all thermally occupied configurations of the reactant state. For two harmonic oscillators with force constants k_1 and k_2

$$\int_R \exp(-\Delta G_{mf}(r)/RT)\, dr = 2\pi RT(k_1 k_2)^{-1/2},$$

where r stands for (r_1, r_2) and the integral is taken over the reactant region R.

We make two assumptions:

1. The proton transfer rate $k_H(r)$ is proportional to the probability density of the (relaxed) *product* state to be at r in the biasing coordinate plane and therefore strongly peaks in a region that we will indicate by $*$. The rationale for this is that the electron redistribution, concerted with proton transfer, yields the product state as the end product of this single reactive step.
2. The potential of mean force ΔG_{mf} is constant within the $*$ region of the biasing coordinate plane. Although not correct, the error introduced by a slope of ΔG_{mf} is negligible compared to the error in ΔG_{mf} itself.

With these assumptions and approximating the product well as two harmonic oscillators with force constants k_1^* and k_2^*, the rate can be expressed as

$$k = \frac{\int_* k_H(r)\exp(-\Delta G_{mf}(r)/RT)\, dr}{\int_R \exp(-\Delta G_{mf}(r)/RT)\, dr} = k_H \sqrt{\frac{k_1 k_2}{k_1^* k_2^*}}\, e^{-\Delta G^*_{mf}/RT}, \quad (1)$$

where ΔG^*_{mf} is the potential of mean force at the reactive (i.e., product) coordinates and k_H is now the proton transfer rate from the $*$ state.

Potential of Mean Force of Biased State

The potential of mean force ΔG^*_{mf} at the product-state coordinates consists of a QM component for the solute and a classical solvent component. For the QM component we use the *in vacuo* energy difference of the reactant state (46.9 kcal/mol, see earlier section), diminished with the energy difference computed in the next section between the proton on the product side and on the reactant side. The *in vacuo* quantum-mechanical component of that energy is 20.1 kcal/mol. Thus, the solute component of ΔG^*_{mf} equals 26.8 kcal/mol.

The solvent part is calculated by TI using MD. The method we used consists of defining harmonic restraining potentials in the biasing coordinate plane for the reactant (R) state and the biased ($*$) state: the chosen harmonic force constants were $k_1 = 67.2$ and $k_2 = 9.0$ kcal mol^{-1} Å^{-2} for R_{CO} and R_{OO} in the R state and $k_1' = k_2' = 3000$ kcal mol^{-1} Å^{-2} for both directions in the $*$ state. The former are values fitted to AM1 calculations; the latter values are arbitrary restraints that confine the bias state but have no influence on the result.

A path, characterized by a *coupling parameter* λ between 0 and 1, was defined. Intermediate points were obtained by linear interpolation of biasing coordinates, force constants, and partial charges. The equilibrated ensemble average at constant temperature and pressure for $\partial V/\partial\lambda$ (V is the potential energy) at any λ yields the derivative of the Gibbs free energy $dG/d\lambda$ at that point.

The result for the Gibbs free energy difference $\Delta G^* = G^* - G^R$ is -13.2 ± 0.4 kcal/mol. If this result is recast in terms of the potential of mean force for the solvent contribution to ΔG^*_{mf}, using

$$\Delta^s G^*_{mf} = \Delta G^* - \frac{1}{2} RT \ln \frac{k_1 k_2}{k_1' k_2'}, \quad (2)$$

where k_1' and k_2' are the force constants of the restraining potential imposed on the $*$ state, we obtain $\Delta^s G^*_{mf} = -16.1 \pm 0.4$ kcal/mol. Hence, the total potential of mean force at the $*$ state is $\Delta G^*_{mf} = 26.8 - 16.1 = 10.7$ kcal/mol. We note that the solvent significantly favors the $*$ state and thus facilitates the reaction.

Biased Proton Reaction Rate

The next step is to compute the proton quantum-dynamical reaction rate k_H from the biased configuration. For this purpose we use a 100-ps dynamic MD run at the $*$ state. The trajectory was saved every 10 fs, which preserves all information available from the MD run. In this classical MD run the proton was modeled as a point charge fixed in the reactant region, which is an excellent approximation for interactions with the environment.[29]

Because the proton transfer rate is small on the time scale of the simulation, we can only derive the initial rate of the reaction. The proton remains in the reactant configuration and no reverse reaction (or barrier recrossing in classical terms) will occur. This has the advantage that the quantum-dynamical part of the calculation can be carried out *a posteriori*.[30]

For each of the 10^4 MD frames the proton potential was determined by taking the solute configuration and putting the proton on 10 different points between the two water oxygens. For each of these 10^5 configurations the solute contribution to the potential V_{solute} was calculated on the AM1 level and to this the classical contribution V_{solvent} was added. Cubic spline interpolation was used to complete the potential curves. All solvent–solute interactions were included, using solute partial charges at several positions of the proton. In this way the complete QM response of the solute to the proton position, including polarizability contributions, was incorporated.

The time evolution of the classical splitting $\Delta E(t)$, defined as the energy difference between the reactant and product states,[31,32] is depicted in Figure 2. Although the *average* proton potential is about 10 kcal/mol higher on the product side without a clear well and thus would not favor proton transfer, Figure 2 shows that on many occasions during the 100-ps simulation a splitting occurs that is zero or even negative. It is these points of the simulation that contribute the most to the rate constant. The use of biased sampling ensured that many of such points did occur during the 100-ps simulation time.

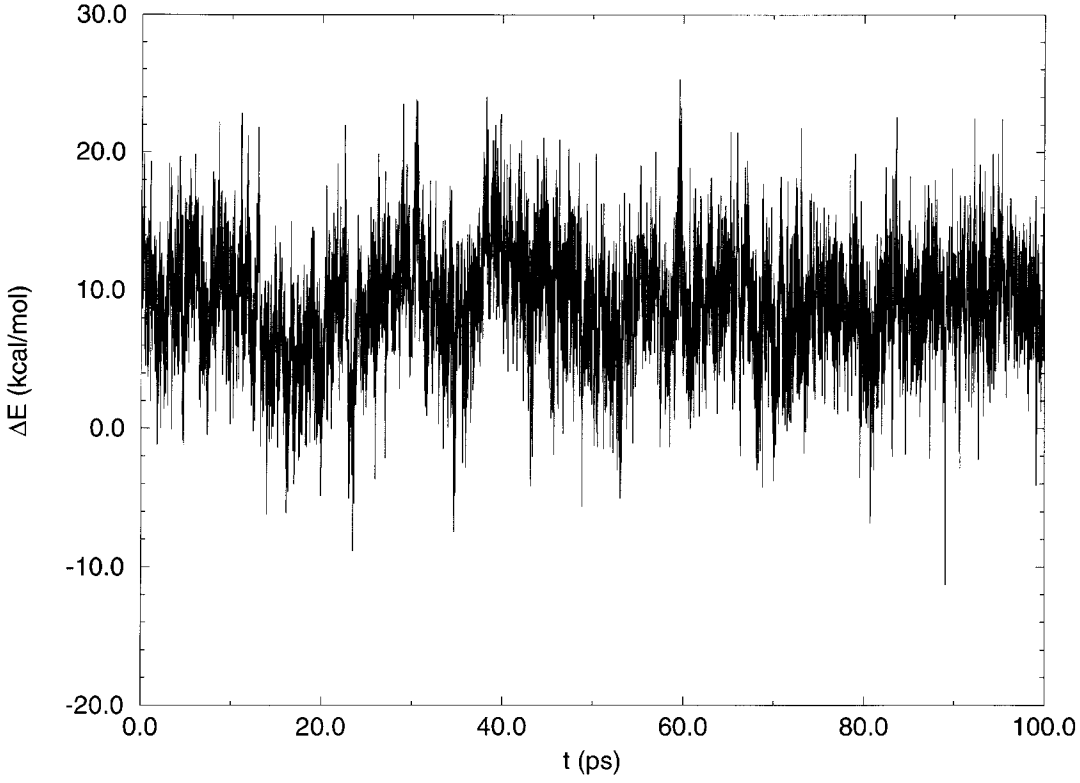

FIGURE 2. Time evolution of the splitting $\Delta E(t)$, defined as the energy difference between the structure with the proton in the product well and the one with the proton in the reactant well.

The normalized probability density $w(\Delta E)$ of the classical energy splitting for the $*$ state (Fig. 2) is shown in Figure 3. The top graph in Figure 3 shows the probability density, the bottom graph the corresponding free energy profile $\Delta G(\Delta E) = -k_B T \log w(\Delta E) + k_B T \log w(\langle \Delta E \rangle)$. It can be seen that the energy splitting has a Gaussian distribution. This is the result of the perturbation coming from many independent sources, because the interaction is mainly electrostatic and thus long ranged. It is remarkable that this quadratic behavior for ΔE, as assumed in Marcus' theory,[33] is in fact observed for proton transfer.[5, 6, 17, 34, 35]

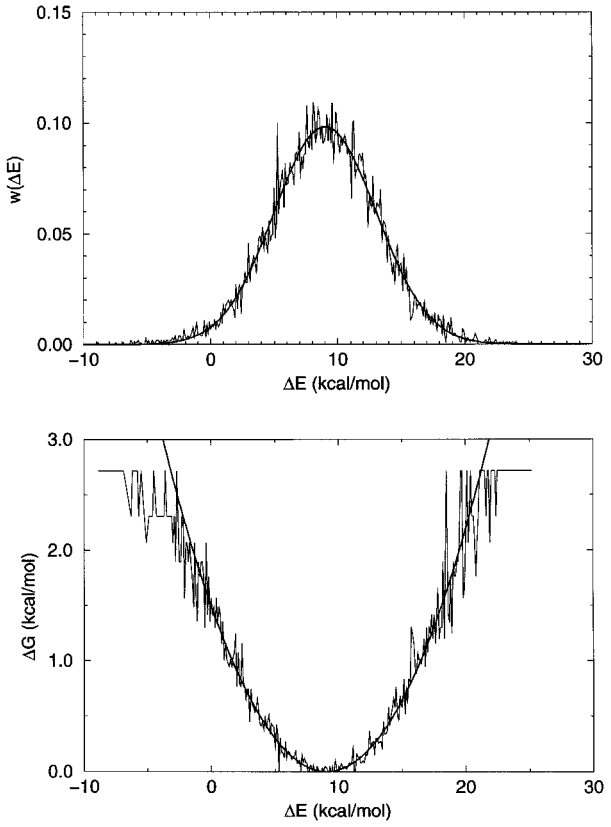

FIGURE 3. The top graph shows the normalized probability density of the energy splitting $w(\Delta E)$, calculated from the 100-ps MD simulation. The thick line is a Gaussian approximation to this. Because the trajectory was saved every 10 fs, this means that the graph is constructed from 10.000 samples. The bottom graph shows the corresponding free energy profile $\Delta G(\Delta E) = -k_B T \log w(\Delta E) + k_B T \log w(\langle \Delta E \rangle)$ for both the simulation data and the Gaussian approximation. The harmonic approximation has a correlation coefficient of 0.93. The anharmonic behavior at the higher free energy points is due to the bad statistics in that area of configurational space.

Note that Figure 3 represents a single well, because in this work only the reactant region is simulated. The curve of Figure 3 provides the probability of zero-energy splitting that could be used in an analytical tunneling rate theory. In this work, however, we include the full fluctuations in the prediction of proton transfer rates.

The QM parts of the proton potentials, calculated in this procedure, gave as an average $\Delta E_{\mathrm{QM}}(t) = -20.1 \pm 3.0$ kcal/mol. This value was used for correction of the QM part of the bias energy (previous section).

With the 100-ps proton potentials in hand, the *time-dependent* Schrödinger equation was solved with the DME method using 750 different starting points. The product state occupation Θ is defined as

$$\Theta(t) = \int_{\xi_{\mathrm{barrier}}}^{\infty} \Psi^*(\xi, t)\Psi(\xi, t)\, d\xi, \qquad (3)$$

where ξ is the proton coordinate and ξ_{barrier} is chosen at the energy barrier for the time-averaged proton potential. Reported values are averaged over all time origins. The coarse-grained slope of the slowly increasing $\langle \Theta \rangle$ (Fig. 4) can then be extrapolated[4, 18] to yield a first-order rate constant $k_H = 2.4 \times 10^7\ \mathrm{s}^{-1}$. The inaccuracy of this value is about a factor of 2 and we conclude that $\log(k_H/\mathrm{s}^{-1}) = 7.4 \pm 0.3$.

In order to calculate the KIE k_H/k_D, the quantum dynamics was recalculated for the deuteron, using the same procedure as for the proton. A rate constant k_D of $0.62 \times 10^7\ \mathrm{s}^{-1}$ was found. We can thus conclude that the calculated KIE is $2.4/0.62 = 3.9$. Within the statistical simulation error this is in excellent agreement with the experimentally observed value of 3.2 ± 0.1.[2]

Overall Reaction Rate

Equation (1) for the overall rate of the reaction consists of a proton transfer rate k_H from the biased state, multiplied by a probability factor p_{bias} for the biased state. Using[36] the values $k_1 = 67.2$, $k_2 = 9.0$, $k_1^* = 973$, $k_2^* = 101$, and the value of 10.7 kcal/mol for ΔG_{mf}^*, we find $p_{\mathrm{bias}} = 1.12 \times 10^{-9}$ or $\log p_{\mathrm{bias}} = -8.95$. The error in this value results largely from the error in the QM terms. Assuming an error of 2 kcal/mol in the potential of mean force, the error in $\log p_{\mathrm{bias}}$ is 1.4. The overall rate becomes $2.7 \times 10^{-2}\ \mathrm{s}^{-1}$ or $\log k = -1.6 \pm 1.6$. This value overestimates the experi-

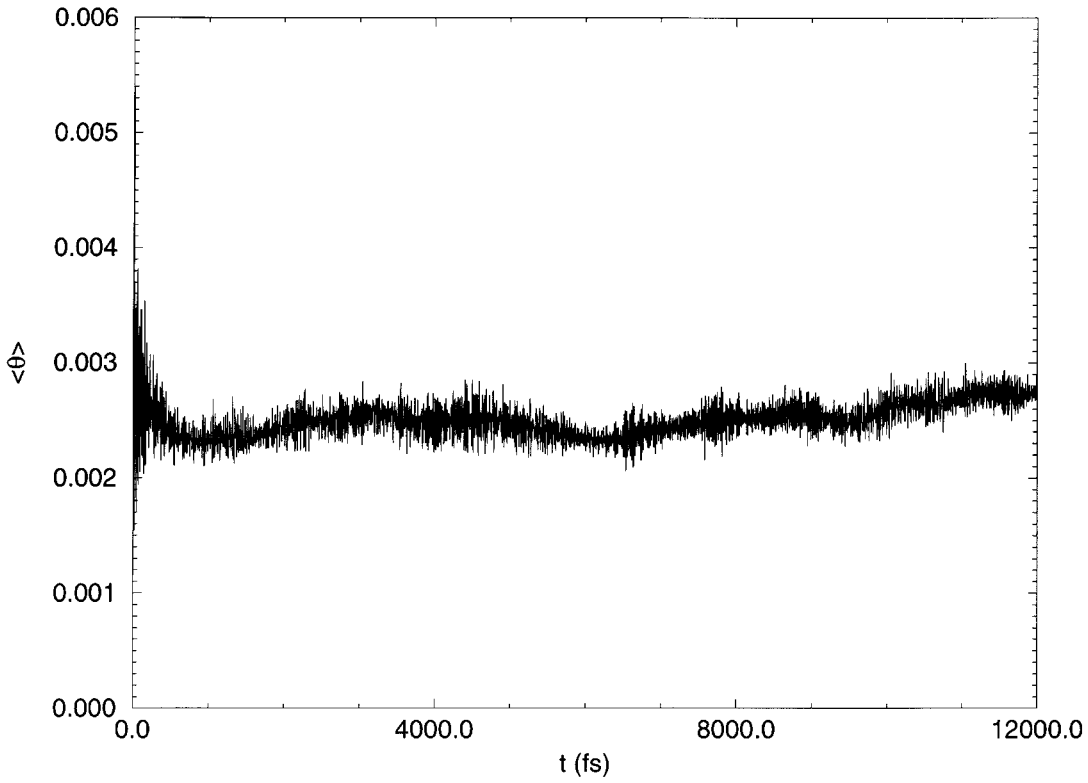

FIGURE 4. Trajectory-averaged evolution of the product state occupation $\Theta(t)$ [see eq. (3)]. The ξ_{barrier} was chosen at 1.40 Å. Extrapolation of the initial rate of transfer leads to $\log k_{\text{bias}} = 7.4 \pm 0.3$ for the biased ester.

mental rate of $\log k_{\text{exp}} = -2.56$ by an order of magnitude, but it still agrees within the error of the calculation.

Discussion and Conclusion

We showed that it is possible to compute the reaction rate of a slow reaction where the rate-limiting step is solvent-induced proton transfer from an activated state, using a combination of semiempirical QM, classical MD, and quantum-dynamical simulations. The simulations give insight into the details of the process and serve to illustrate the inadequacy of standard transition-state theory for such processes. The overall picture is that the system ''waits'' until a fluctuation allows the occurrence of a biased state ($*$) from which proton transfer takes place in a nonadiabatic process. This is illustrated in Fig. 5. We note that the $\pm$ state indicated in Fig. 5 is not relevant for the neutral hydrolysis reaction because it involves an OH^- ion as an intermediate, which occurs in fact in the base-catalyzed hydrolysis observable at higher pH.

The occurrence of the $*$ state can be described by classical statistical mechanics as in transition state theory (TST), but the proton transfer has an essential quantum character and is driven by a fluctuating potential due to the environment. Analytical theories for this process exist only in the two-state approximation.[4, 31] The Gibbs free energy of the $*$ state is considerably stabilized by the orientational polarization of the aqueous environment. Applying straightforward TST to the proton transfer (assuming an AM1-SM1 calculated barrier of 7.1 kcal/mol and a proton zero point energy of 1.75 kcal/mol as calculated from the average proton potential, and including the bias probability p_{bias} as computed above), we find a rate constant of 0.8 s^{-1} and a KIE of 2.4. This overestimates the experimental rate by more than two orders of magnitude and underestimates the KIE.

The DME method is quite suitable to simulate the initial rate of the reaction where the proton interacting with its classical environment can be approximated as a classical particle and where backreaction due to the proton quantum dynamics onto its environment can be neglected. The ques-

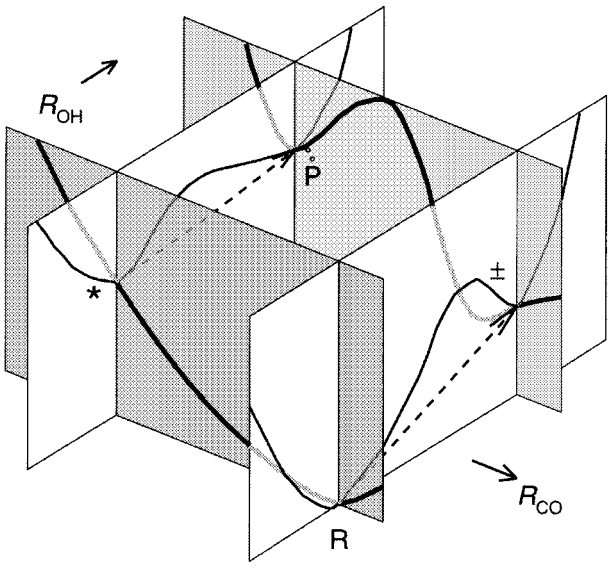

FIGURE 5. Sketch of the free energy diagram for the neutral hydrolysis reaction. The simplified coordinate R_{CO} represents both biasing coordinates R_{CO} and R_{OO}; R_{OH} represents the reaction coordinate along which the proton transfer takes place. The concerted reaction proceeds via the $*$ state. The $\pm$ state refers to a reaction pathway via a hydroxyl ion, which we consider of negligible importance for the neutral hydrolysis reaction.

tion of whether it is correct to use Hellmann–Feynman forces from mixed states or whether surface hopping[7] should be introduced does not come up in this case. The complete proton transfer, which occurs only once in several tens of nanoseconds, cannot be directly simulated at present. Therefore, it is also not yet possible to compute the barrier recrossing ratio (i.e., the fraction of unsuccessful transfers), which is expected to reduce the rate by a factor of about 2.[5, 6, 35]

We made restrictions in the position of the water molecule nearest to the carbonyl, constraining it to a region above the carbon atom, perpendicular to the ester plane. This restriction was not further investigated and was not incorporated into the probability of the $*$ state. It will lead to a negative entropic contribution to the transition state and an overestimation of the rate constant. If we estimate this to be a factor of 10 (a water molecule must reside in about 1 Å^2 of surface area of the 10 Å^2 available to it), its inclusion would lead to perfect but fortuitous agreement with the experiment. It is likely, however, that the entropic factor related to the probability that a water molecule occupies the required position forms the basis for solvent effects on the reaction rate in mixed solvents. Work addressing both these aspects (i.e., the entropic contribution of a water molecule residing in proximity to the ester or not, as well as the influence of cosolvents) is in progress.

A disputable point in the present treatment is the assumption that the $*$ state has a sufficient lifetime to allow proton transfer to take place. However, there is no need for the $*$ state to persist over tens of nanoseconds, which is the average time it takes until a transition occurs. In fact, it should live a much shorter time for the presumed preequilibrium between the initial and $*$ state to be valid. But the $*$ state should persist over the duration of an actual proton transfer, which is less than 1 ps.[19] The treatment could be refined by incorporating the motion of the biasing coordinates into the quantum dynamics, but then a bias should be introduced into the initial quantum conditions to make the transition observable. If this can be done in a reliable way, the backreaction can be included as well.[10]

While classical MD of complex systems has already come of age,[37] the embedding of semiempirical QM and quantum dynamics in classical MD broadens applications to reactive pathways, even on time scales far beyond the brute-force application of these methods.

Acknowledgments

This work was performed at the Centre Européen de Calcul Atomique et Moléculaire (CECAM) in Lyon, France. We wish to thank Giovanni Ciccotti and Stefano Baroni for hospitality at CECAM. J. M. is grateful for a long-term HFSP stipend and to the University of Groningen for the hospitality during his stay in Groningen. We are grateful to Jan Engberts, University of Groningen, for stimulating initial discussions and arousing our interest in this reaction.

References

1. Isaacs, N. S. Physical Organic Chemistry; Longman: New York, 1987.
2. (a) Engbersen, J. F. J.; Engberts, J. B. F. N. J Am Chem Soc 1974, 96, 1231; (b) Engbersen, J. F. J.; Engberts, J. B. F. N. J Am Chem Soc 1974, 97, 1563; (c) Holterman, H. A. J.; Engberts, J. B. F. N. J Am Chem Soc 1980, 102, 4256; (d) Holterman, H. A. J.; Engberts, J. B. F. N. J Org Chem 1983, 48, 4025.
3. (a) Mezei, M.; Beveridge, D. L. Ann NY Acad Sci 1986, 582, 1; (b) Van Gunsteren, W. F.; Berendsen, H. J. C. Angew Chem Int Ed Engl 1990, 29, 992.

4. (a) Berendsen, H. J. C.; Mavri, J. J Phys Chem 1993, 97, 13464; (b) Mavri, J.; Berendsen, H. J. C. J Mol Struct 1994, 322, 1; (c) Mavri, J.; Berendsen, H. J. C. J Phys Chem 1995, 99, 12711; (d) Berendsen, H. J. C.; Mavri, J. In Quantum Mechanical Simulation Methods for Studying Biological Systems; Bicout, D.; Field, M., Eds.; Springer-Verlag: Berlin, 1996; p 157.
5. (a) Azzouz, H.; Borgis, D. J Chem Phys 1993, 98, 7361; (b) Staib, A.; Borgis, D.; Hynes, J. T. J Chem Phys 1995, 102, 2487.
6. Laria, D.; Ciccotti, G.; Ferrario, M.; Kapral, R. J Chem Phys 1992, 97, 378.
7. (a) Tully, J. C. J Chem Phys 1990, 93, 1061; (b) Coker, D. F. In Computer Simulation in Chemical Physics; Allen, M. P.; Tildesley, D. S., Eds.; Kluwer Academic: Boston, 1993; p 315; (c) Hammes–Schiffer, S.; Tully, J. C. J Chem Phys 1994, 101, 4657; (d) Coker, D. F.; Xiao, L. J Chem Phys 1995, 102, 496.
8. (a) Topaler, M.; Makri, N. Chem Phys Lett 1993, 210, 285; (b) Makarov, D. E.; Makri, N. Phys Rev A 1993, 48, 3626.
9. (a) Cao, J.; Voth, G. A. J Chem Phys 1993, 99, 10070; (b) Cao, J.; Voth, G. A. J Chem Phys 1994, 100, 5106; (c) Lobaugh, J.; Voth, G. A. J Chem Phys 1996, 104, 2056.
10. Hammes–Schiffer, S.; Tully, J. C. J Chem Phys 1995, 103, 8528.
11. Chandrasekhar, J.; Smith, S. F.; Jorgensen, W. L. J Am Chem Soc 1985, 107, 154.
12. (a) Van Duijnen, P. T.; Thole, B. T.; Broer, R.; Nieuwpoort, W. C. Int J Quantum Chem 1980, 17, 651; (b) Rullmann, J. A. C.; Bellido, M. N.; Van Duijnen, P. T. J Mol Biol 1989, 206, 101.
13. (a) Warshel, A. J Phys Chem 1982, 86, 2218; (b) Warshel, A.; Chu, Z. T. J Chem Phys 1990, 93, 4003.
14. Maraver, J. J.; Marcos, E. S.; Bertran, J. J Chem Soc Perkin Trans 1986, 8, 1323.
15. Tomasi, J.; Persico, M. Chem Rev 1994, 94, 2027.
16. Lu, D.; Voth, G. A. J Am Chem Soc 1998, 120, 4006.
17. Mavri, J.; Berendsen, H. J. C.; Van Gunsteren, W. F. J Phys Chem 1993, 97, 13469.
18. Mavri, J.; Berendsen, H. J. C. J Phys Chem 1995, 99, 12711.
19. (a) Bala, P.; Grochowski, P.; Lesyng, B.; McCammon, J. A. J Phys Chem 1996, 100, 2535; (b) Bala, P.; Grochowski, P.; Lesyng, B.; McCammon, J. A. In Quantum Mechanical Simulation Methods for Studying Biological Systems; Bicout, D.; Field, M., Eds.; Springer-Verlag: Berlin, 1996; p 119; (c) Grochowski, P.; Lesyng, B.; Bala, P.; McCammon, J. A. Int J Quantum Chem 1996, 60, 1143.
20. (a) Stewart, J. J. P. QCPE Bull 1990, 10, 86; (b) Jones, J. P. MOBOSOL; Departments of Chemistry and Pharmacology, University of Rochester: Rochester, NY.
21. Frisch, M. J.; Trucks, G. W.; Schlegel, H. B.; Gill, P. M. W.; Johnson, B. G.; Wong, M. W.; Foresman, J. B.; Robb, M. A.; Head–Gordon, M.; Replogle, E. S.; Gomperts, R.; Andres, J. L.; Raghavachari, K.; Binkley, J. S.; Gonzalez, C.; Martin, R. L.; Fox, D. J.; Defrees, D. J.; Baker, J.; Stewart, J. J. P.; Pople, J. A. Gaussian 92/DFT, Revision G.1; Gaussian Inc.: Pittsburgh, PA, 1993.
22. Van Gunsteren, W. F.; Berendsen, H. J. C. GROMOS, Groningen Molecular Simulation Package; Biomos B.V.: Groningen, The Netherlands, 1987.
23. Berendsen, H. J. C.; Postma, J. P. M.; Van Gunsteren, W. F.; Hermans, J. In Intermolecular Forces; Pullman, B., Ed.; Reidel: Dordrecht, 1981; p 331.
24. Berendsen, H. J. C.; Postma, J. P. M.; DiNola, A.; Haak, J. R. J Chem Phys 1984, 81, 8.
25. Ryckaert, J. P.; Ciccotti, G.; Berendsen, H. J. C. J Comput Phys 1977, 23, 327.
26. Cramer, C. J.; Truhlar, D. G. J Am Chem Soc 1994, 116, 3892.
27. Bessler, B. H.; Merz, K. M. Jr.; Kollman, P. A. J Comput Chem 1990, 11, 431.
28. (a) Dewar, M. J. S.; Zoebisch, E. G.; Healy, E. A.; Stewart, J. J. P. J Am Chem Soc 1985, 107, 3902; (b) Cramer, C. J.; Truhlar, D. G. J Comput Aided Mol Design 1992 6, 629.
29. Berendsen, H. J. C.; Mavri, J. Int J Quantum Chem 1996, 57, 975.
30. This is the ZBR (zero backreaction) approximation: the force exerted by the quantum subsystem on the classical environment is independent of the quantum state. See Xiao, L.; Coker, D. F. J Chem Phys 1995, 102, 1107.
31. Borgis, D.; Hynes, J. T. J Chem Phys 1991, 94, 3619.
32. The proton was considered at R_{OH} distances of about 1.0 and 1.5 Å, the exact coordinates depending on the location of the reactant and product wells.
33. Marcus, R. A.; Sutin, N. Biochim Biophys Acta 1985, 811, 265.
34. (a) Kuharski, R. A.; Bader, J. S.; Chandler, D.; Sprik, M.; Klein, M. L.; Impey, R. W. J Chem Phys 1988, 89, 3248; (b) Borgis, D.; Tarjus, G.; Azzouz, H. J Phys Chem 1992, 96, 3188.
35. Consta, S.; Kapral, R. J Chem Phys 1996, 104, 4581.
36. The values of k_1 and k_2 are immaterial, because they cancel in eqs. (1) and (2).
37. Berendsen, H. J. C. Science 1996, 271, 954.